Journal of
Ceramic Science
and Technology

J. Ceram. Sci. Tech., **04** [02] 59-68 (2013)
DOI: 10.4416/JCST2012-00035
available online at: http://www.ceramic-science.com
© 2013 Göller Verlag

The Effect of Different La-Containing Starting Materials on the Synthesis, Sintering, and Li^+-Conductivity of $Li_{3x}La_{2/3-x}TiO_3$

A.C. Sutorik*[1], C. Cooper[1], M.D. Green[1], J. Wolfenstine[2], G. Gilde[1]

[1]U.S. Army Research Laboratory, RDRL WMM E, Building 4600, Aberdeen Proving Ground, D 21005, USA
[2]U.S. Army Research Laboratory, RDRL SED C, 2800 Powder Mill Road, Adelphi, MD 20783, USA
received September 20, 2012; received in revised form November 1, 2012; accepted November 9, 2012

Abstract

$Li_{3x}La_{2/3-x}TiO_3$ is a promising ceramic electrolyte for high energy density Li-batteries. The material is usually prepared from solid state reactions between Li_2CO_3, La_2O_3, and TiO_2, but the hydroscopic nature of La_2O_3 leads to inconsistencies in formulation and synthetic outcome which can impact the phase formation and corresponding Li-conductivity of the final ceramic. To address this issue, La carbonate and hydroxides have been evaluated as starting materials for solid state synthesis of $Li_{3x}La_{2/3-x}TiO_3$ powders and sintered ceramic. The different La-starting materials are all prepared from precipitation reaction as high surface area powders. These are characterized for phase, particle size, particle morphology, and ceramic yield (by thermal gravimetric analysis). The La starting materials are then mixed with the desired stoichiometric amounts of Li_2CO_3 and TiO_2. The mixtures are calcined at 1100 °C for 1 h before being pressed into green parts and sintered at either 1200 or 1300 °C for 6 h. Under nearly all conditions investigated, the formulations using the La-carbonate-based starting material lead to ceramics with the highest bulk density, the highest degree of cubic superstructure formation, and the highest lattice Li^+-conductivity. Total conductivity, however, appears largely insensitive to the La starting material used.

Keywords: *Li^+-conducting ceramic, Li-air battery, ceramic electrolyte, lithium lanthanum titanate*

I. Introduction

In lithium-air batteries, metallic lithium serves as the anode and O_2, diffusing from the atmosphere through a porous or semi-permeable support, acts as the cathode [1]. The design offers the potential for high theoretical specific energy densities which are estimated to range from 3000 – 10000 Wh/kg, depending on design and efficiency assumptions [2,3,4]. The low end of this range is a full order of magnitude above the current state of the art for Li-batteries. Because of the high reactivity of the Li metal anode, the design requirements for device integrity, safety, and stability are very high, particularly if a rechargeable battery is desired, and conventional electrolyte systems typically do not meet these criteria. Several groups have explored novel electrolyte systems for use with metallic Li anodes, such as gel electrolytes with non-volatile plasticizers [5], ionic liquids [6], and laminate structures made of separate glass-ceramic and polymer-ceramic composites [3].

Solid state ceramic electrolytes would offer unique advantages in this application because of the combination of several desirable properties such as fast lithium ion transport, impermeability towards liquid co-electrolytes, low electronic conductivity, high mechanical strength, and excellent chemical stability [7,8]. The strategy allows for the use of co-electrolytes to enhance both Li^+ transport and cell stability, because, due to the impermeable solid state separator, different liquid electrolytes can be used which are optimal to the needs of the different electrodes (i.e. non-aqueous for contact with the Li metal anode and aqueous for diffusion of O_2 cathode) [1]. One of the challenges in optimizing candidate ceramic electrolytes is that their ionic conductivity is typically characterized by two parameters: the lattice conductivity, which describes the Li^+ conductivity within the crystal structure, and the total conductivity, which includes grain boundary resistance. The former serves as a theoretical maximum for a given sample and is typically governed by the intrinsic chemistry and crystal structure. The total conductivity is what would be manifest in the workings of an actual electrochemical device, and this is a function of impurities (or lack thereof) at the grain boundaries, the amount of residual porosity in the ceramic (i.e. maximized grain to grain contact) and grain size. For optimized device performance, total conductivity should be as close to lattice conductivity as possible. As such, control of both ceramic powder synthesis and subsequent sintering to full density should be studied in tandem to achieve consistently optimized and reproducible lattice and total conductivity for a ceramic electrolyte.

Lithium Lanthanum Titanate (LLTO) (stoichiometry $Li_{3x}La_{(2/3)-x}TiO_3$) is a perovskite-based Li^+-conducting ceramic under consideration as a ceramic electrolyte for Li-air batteries [9], as well as other advanced battery ap-

* Corresponding author: anthony.sutorik1@us.army.mil

plications such as all-solid state Li-ion batteries [10,11]. One reason for the interest in LLTO is that among Li^+ conducting ceramics it has some of the highest reported values for room temperature lattice conductivities at ~ $1.0 \cdot 10^{-3}$ S/cm [12,13]. Additionally important for this application is that the material has a high stability in aqueous environments [9]. LLTO has been the subject of considerable study in order to understand the major chemical and structural factors contributing to optimized conductivity [13]. The highest lattice conductivity can be attained when x ~ 1.0, but this is not guaranteed solely on the basis of composition. For these stoichiometries, LLTO can primarily form one of two polymorphs. The high temperature form, which is typically stabilized by rapid quenching from > 1150 °C, is nearly an ideal ABO_3 cubic perovskite structure with Li^+ and La^{3+} cations randomly distributed among the A-cation sites. When slow-cooled or annealed at lower temperatures, the Li^+ and La^{3+} cations segregate into alternating layers of the A-site oriented perpedicular to the c-axis; this ordering manifests itself as a doubling of the c-axis (relative to the idealized cubic perovskite structure), a slight shrinking of the a-axis, and the occurence of tetragonal superstructure peaks in the powder diffraction pattern [13]. The lattice distortion in the formation of the tetragonal superstructure leads to restrictions in the Li^+ conduction pathways which in turn decrease Li^+ lattice conductivity. The transition between the two phases is not always sharp, and the degree of cation ordering giving rise to the tetragonal superstructure can be determined based on the relative intensity of the characteristic peaks in powder X -ray diffraction experiments. As a guiding prinicple, the higher the degree of cubic character to the superstructure (and concurrently, the lower the degree of tetragonal character), the higher the Li^+ lattice conductivity.

Most commonly LLTO powders are prepared from the direct solid state reaction of Li_2CO_3, La_2O_3, and TiO_2 at > 1150 °C for extended periods of time (> 24 h) and through one or more regrinding and refiring steps. This adds a further complication to the reaction since Li loss, due to Li_2O volatilization at high temperatures, can reach as high as 20 % [14] and could retard Li^+-conductivity through a reduced number of carriers. Typically, Li loss is accounted for by addition of an empirically determined excess of Li_2CO_3, and once sintered to a high density, Li^+-conductivity of LLTO appears fairly insensitive to either repeated thermal annealing cycles [15] or extended sintering times [16]. As alternatives to the high temperatures of solid state reactions, solution-derived methods to prepare LLTO have also been explored. Wöhrle *et al.* [17] and Kitaoka *et al.* [18] prepared LLTO via sol-gel synthesis using Ti-alkoxides and soluble Li^+ and La^{3+} organic salts, but the products still required calcining at 1300 °C to form phase-pure LLTO. Pham *et al.* have developed a Pechini-style synthesis of pre-ceramic polyesters which under the proper synthetic conditions results in the formation of phase-pure LLTO at as low as 350 °C [19]. These methods are somewhat limited by difficulties associated with scale-up or the expense of starting materials, and so solid state reactions are still preferred for the synthesis of the 100-s of grams of LLTO powder needed for device research and development, particularly since the issues of Li^+ loss can be ameliorated.

Considered to a much lesser degree in the open literature has been the influence of the nature of the TiO_2 and La_2O_3 starting materials. For example, the phase identity of the TiO_2 starting material, whether anatase, rutile, or a mixture thereof, is rarely stated, and so its potential influence on the reaction outcome is unknown. The nature of the TiO_2 polymorph was recently found to have a significant impact on the formation of $Li_4Ti_5O_{12}$ from solid state reaction [20]. La_2O_3 presents its own challenges in that the material is hygroscopic to the extent that if left open to the atmosphere for extended periods the oxide will chemisorb a significant amount of moisture, converting, in part or in total, to $La(OH)_3$. Procedures to guard against this occurence are often alluded to in published reports. For example, starting powders are heated before use and stored in a moisture-free environment if not used immediately. However, the rapidity with which the hydrolysis takes place raises concerns that unless careful procedures are consistently applied, chance contamination of starting material or systemic contamination on prolonged storage may be a source of significant synthetic error. This could have a consequence in stoichiometric reproducibility, as the amount of hydrolytic contamination could vary with exposure, or could present sources of sintering inhomogeneity and residual porosity if hydroxide is not completely and uniformly removed before the ceramics achieve a significant amount of closed porosity. In order to have a more stable starting material to use for large-scale reactions, several alternative La-containing starting materials were prepared, and their impact on LLTO phase formation, ceramic density, and conductivity (both lattice and total) was studied.

II. Experimental

(1) Starting materials

The following were used as-received in the described syntheses: Li_2CO_3 (99.0 %, Alfa Aesar, Ward Hill, MA, USA); La_2O_3 (99.99 %; PIDC, Ann Arbor, MI, USA); TiO_2 (99.8 % Alfa Aesar, Ward Hill, MA, USA); HNO_3 (68 – 70 %, A.C.S. reagent grade, Mallinckrodt, Phillipsburg, NJ, USA.); NH_4OH (28 – 30 %, A.C.S. reagent grade, Sigma-Aldrich, St Louis, MO, USA), HCl (37 %, A.C.S. reagent grade, Sigma-Aldrich, St Louis, MO, USA), NaOH (97 %, A.C.S. reagent grade, Sigma-Aldrich, St Louis, MO, USA). The amount of moisture and other volatile impurities were determined for TiO_2 by a loss-on-ignition procedure in which 1 – 2 g of sample was loaded into alumina crucibles, and sample masses were determined before and after firing under a ramp rate of 5 °C min^{-1} to 900 °C with a 1-h hold. For La_2O_3, the ceramic yield was determined by means of thermogravimetric analysis (described below) under flowing N_2 to prevent re-absorption of atmospheric moisture on cooling. The results from the ceramic yield determinations were used as correction factors in the stoichiometric calculations.

(2) La starting materials synthese

Lanthanum Hydroxide Nitrate Hydrate, $La(OH)_2NO_3{\cdot}xH_2O$ – 50 g of La_2O_3 was added to 200 g of stirring deionized water. 58.4 mL of concentrated HNO_3 was added slowly to dissolve the La_2O_3 to a nearly clear solution. The solution was vacuum-filtered through a nitrocellulose filter with 0.2 μm particle retention to remove insoluble residue. To the stirring solution was added 80 mL of concentrated NH_4OH, producing a white, fine precipitate. Stirring was continued for 1 h after the addition, and the precipitate was recovered by means of vacuum filtration using nitrocellulose filters with 0.2 μm particle retention. The precipitate cake was redispersed in 500 g of deionized water, and the slurry was stirred for several hours. The solid was again collected by filtration, and the washing was repeated with two more 500 g portions of deionized water. The solid was recovered and dried under dynamic vacuum until water was completely removed (~2d). Powder X-ray diffraction revealed $La(OH)_2(NO_3){\cdot}H_2O$ (PDF# 46 – 346) as the sole crystalline product. To account for excess physisorbed water, the ceramic yield was determined by means of thermal gravimetric analysis as described below.

Lanthanum Trihydroxide, $La(OH)_3$ – 25 g of La_2O_3 was dispersed in 200 g of stirring deionized water. 40.8 mL of concentrated HCl was added slowly to dissolve the La_2O_3 to a clear solution. The solution was vacuum-filtered through a nitrocellulose filter with 0.2 μm particle retention to remove insoluble residue. To the stirring La^{3+} solution was added a solution of 18.91 g of NaOH dissolved in 100 g deionized water, and a fine, white precipitate immediately formed. After stirring for 1 h, the precipitate was recovered by vacuum filtration and washed five times with 400 mL portions of deionized water, as described above. The precipitate was left in a loosely covered container for several days to completely air dry. Powder X-ray diffraction revealed $La(OH)_3$ (PDF# 36 – 1481) as the sole crystalline product. To account for excess physisorbed water, the ceramic yield was determined by means of thermal gravimetric analysis as described below.

Lanthanum Carbonate Hydrate, $La_2(CO_3)_3{\cdot}xH_2O$ – 25 g of La_2O_3 was dispersed in 200 g of stirring deionized water. 40.8 mL of concentrated HCl was added slowly to dissolve the La_2O_3 to a nearly clear solution. The solution was vacuum-filtered as above. A solution of 26.98 g of Na_2CO_3 (10 % stoichiometric excess) dissolved in 100 g deionized water was added to the stirring La^{3+} solution, producing a white, fine precipitate. After stirring for 1 h, the precipitate was recovered by means of vacuum filtration and washed five times with 400 mL portions of deionized water, as described above. The precipitate was left in a loosely covered container for several days to completely air dry. Powder X-ray diffraction revealed $La_2(CO_3)_3{\cdot}8H_2O$ (PDF# 25 – 1400) as the sole crystalline product. Thermal gravimetric analysis was used to determine the full amount of physisorbed moisture remaining on the material in excess of the eight waters of hydration in the crystalline formula.

(3) LLTO powder synthesis and sintering

Combinations of Li_2CO_3, TiO_2, and the desired La-containing starting material were slurry-mixed via magnetic stirring in amounts necessary to form one of two compositions, $Li_{0.29}La_{0.57}TiO_3$ or $Li_{0.35}La_{0.55}TiO_3$, which in the general formulation correspond to $x = 0.097$ and $x = 0.117$, respectively. No other dispersants or additives were employed. When La_2O_3 was used, the slurry was prepared using ethanol which had been stored over water-absorbing molecular sieves. Slurry formulations based on all other La starting materials used simple deionized water. The slurries were prepared at 30 – 40 wt% solids loading (based on starting materials) with intended yields of 25 – 100 g LLTO. The slurries were stirred for approximately 1 – 2 h to homogenize. Once mixed, the slurry was transferred to a rotary evaporator where the bulk of the solvent was removed. The powder mixture was coarsely broken and transferred to a clean, loosely covered container where it was left to stand for a period of one to two days to allow for complete solvent volatilization. After drying, the powder was sieved through a 58-mesh nylon screen and calcined in a high alumina crucible under ambient atmosphere in a closed box furnace. Samples were heated at 5 °C min^{-1} to 1100 °C, held at that temperature for 1 h, and cooled back to room temperature at 5 °C min^{-1}.

LLTO powders were pressed into pellets in a 13-mm diameter stainless steel die with a uniaxial hydraulic press. Each sample was pressed under 68 MPa for approximately 10 s. Green samples were subjected to further consolidation using a cold isostatic press under 207 MPa pressure. Samples were packed in a bed of sacrificial LLTO powder inside alumina crucibles, and sintering was performed under ambient atmosphere in a closed box furnace. Samples were heated to 1200 °C or 1300 °C at 5 °C min^{-1}, held there for 6 h, and cooled at a rate of 5 °C min^{-1}.

(4) Characterization methods

Ceramic yields of all La-containing starting materials were determined by means of thermogravimetric analysis using a TA Q9000 Thermal Analyzer. Approximately 10 – 20 mg of sample was used for each trial. Samples were heated under flowing N_2 at a rate of 10 °C/min to 1000 °C. The ceramic yield was determined from the total mass lost from room temperature to 1000 °C, and the average of three trials for each material was taken to be used in subsequent stoichiometric calculations.

Particle size distributions for synthesized powders were measured using a Horiba LA-910 Light Scattering Particle Size Distribution Analyzer. Samples were prepared by pre-dispersion of 0.1 g powder into 10 g of deionized water with the container immersed in an ultrasonic bath (Li_2CO_3 was dispersed in ethanol). Samples were added drop-wise to a blanked sample holder containing deionized water under magnetic stirring until instrument response fell into the optimum measurement range. Values of D_{50} and D_{90} are reported on a volume distribution basis.

The surface area of starting and synthesized powders was measured using a computer-controlled Micromerit-

ics ASAP 2010 using an 11-point BET analysis protocol. One gram of sample was loaded into a dry sample tube and stored open in a dynamic vacuum furnace at 75 °C overnight to ensure physisorbed species were removed from the samples' surface. Nitrogen gas was used for the adsorbing agent.

Powder X-ray diffraction analysis was employed to determine the crystalline phases in the starting powders, calcined LLTO, and sintered LLTO ceramics. Powders of sintered pellets were prepared by grinding fragments in a glass mortar and pestle to avoid crystalline contamination. Measurements were taken using a computer-controlled Rigaku Minflex operating at 30 kV and 15 mA with a step size of 0.03° 2θ and scan rate of 5° 2θ/min, scanning over 5 – 60°. Powder samples were loaded directly into low-background amorphous Si sample holders.

A Hitachi 4700 Scanning Electron Microscope was used to observe the morphology of starting powders, synthesized LLTO powders, and sintered ceramic grain structure. An accelerating voltage of 2 kV and beam current of ~ 10 mA were used throughout this procedure to minimize charging. Samples were applied to double-sided carbon tape and attached to an aluminum sample holder.

The Archimedes method was used to determine the bulk density of the sintered pellets. Each pellet was first weighed to obtain the dry mass. They were then placed under vacuum in a closed vessel for 1 h. The vessel was backfilled with de-ionized water, and samples were left submerged for a few minutes to allow absorption of water into any available open porosity. The pellets were removed and wiped with a damp cloth to remove residual surface water. The wet pellets were then weighed immediately (before significant water evaporation could occur) in air (wet mass) and in a water-submerged basket (submerged mass) using a Mettler Toledo AX205 balance. Using these values, the bulk densities (ρ_{Bulk}) were calculated as follows:

$$\rho_{Bulk} = \left(\frac{m_{dry}}{m_{wet} - m_{submerged}} \right) \rho_{H_2O}$$

where *m* is the mass of the dry, wet, and submerged pellet (as noted in the subscript) and ρ_{H2O} is the density of water.

Samples were prepared for electrochemical characterization by applying a gold coating of ~ 50 nm to the electrode contact surfaces with a Denton Desk IV vacuum cold-sputtering/etch unit. Dimensions of the samples were measured using a Vernier caliper. Averages of five diameter and five width measurements from opposing points around the pellets were used in subsequent calculations. A Solatron SI 1287 Electrochemical Interface was used to measure the AC impedance of the LLTO samples [21, 22]. All samples were measured under a 100mV AC potential, from an initial frequency of 1.0×10^6 Hz to a final frequency of 1.0 Hz using a logarithmic scale in a Teflon sample holder. All measurements were conducted in a dry-room with negligible humidity at room temperature. Electronic resistance of each of the samples was measured using a Keithly 6517A High Resistance Electrometer with 8009 Resistivity Test Fixture. All samples were left overnight in the test fixture and final electronic resistivity was reported from the equilibrated value.

III. Results and Discussion

Rather than source multiple La-containing starting materials from different suppliers, the decision was made to prepare simple La salts in-house from the same La_2O_3 source. This approach reduces the risk of variability by retaining control over as many factors of synthesis as possible. Additionally, the targeted starting materials were chosen because they would not be a source of carbonaceous contamination during solid state reaction (as would organic salts such as oxalates or acetates) and because they should not be prone to moisture absorption from the atmosphere. The synthesis of $La(OH)_2(NO_3)\cdot xH_2O$ was actually unintended; the intended product was $La(OH)_3$, but the full exchange reaction of hydroxide for nitrate did not occur. Rather than discard the mixed hydroxide/nitrate, it was incorporated into our LLTO study, and the full hydroxide was alternately prepared from a chloride solution as described.

Table 1: Measured surface area and particle size distributions of as-prepared La starting materials.

	Surface area /m^2/g	Size distribution by dynamic light scattering	
		D_{50}/ μm	D_{90}/μm
$La_2(CO_3)_3\cdot 8H_2O$	9.71 ± 0.17	10.5 ± 0.6	20.5 ± 1.0
$La(OH)_3$	76.9 ± 0.4	9.2 ± 0.4	113.1 ± 16.1
$La(OH)_2(NO_3)\cdot xH_2O$	19.8 ± 0.2	7.4 ± 2.6	50.4 ± 9.6
La_2O_3	3.95 ± 1.06	14.1 ± 1.1	37.9 ± 6.8

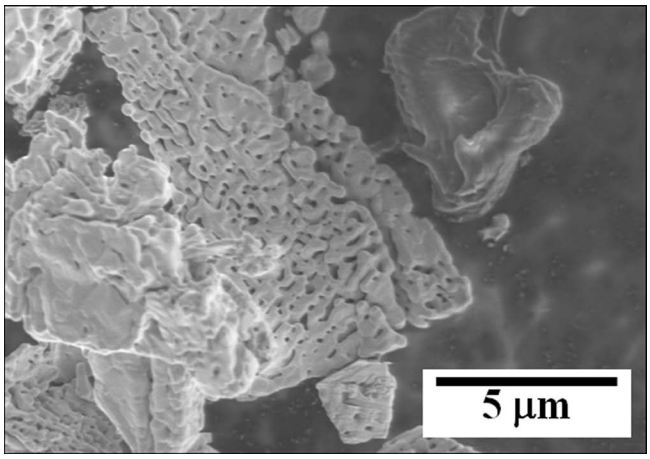

Fig. 1: Representative electron micrograph of La_2O_3 starting powder.

The results of surface area measurements and particle size analysis by means of dynamic light scattering are given in Table 1. The agglomerate sizes estimated from the light scattering measurements are generally confirmed by the scanning electron micrographs (SEMs), which also provide more detail about the primary particle size and morphology. La_2O_3 appears porous and heavily necked (Fig. 1), which likely has consequences for the reactivi-

ty and subsequent sintering of LLTO produced from it. Both the mixed hydroxide/nitrate and the trihydroxide are high-surface-area powders where the primary particles are in the 100s of nanometers; these then form agglomerates over a broad size distribution (Fig. 2). The morphology of $La_2(CO_3)_3{\cdot}xH_2O$ particles is of two-dimensional plates (Fig. 3). These form agglomerates whose D_{50} is higher than that of the hydroxide-containing materials, but the size distribution is much narrower in that the D_{90} is only approximately twice the D_{50}. Although variations in particle morphology could have implications for optimized reactivity, for the purposes of material screening, the La starting materials were used in their as-prepared form without additional particle size refinement.

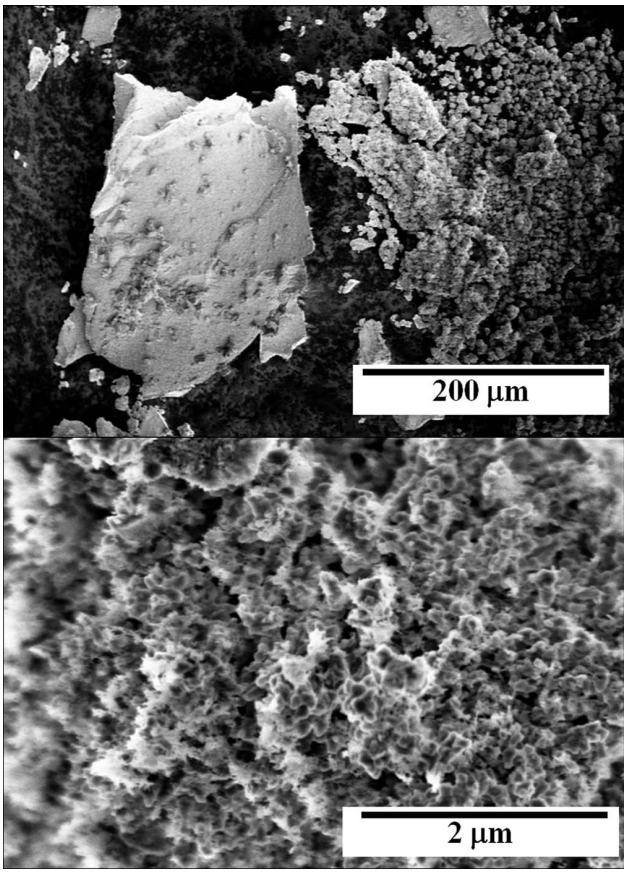

Fig. 2: Representative electron micrographs of as-prepared $La(OH)_3$ starting powder.

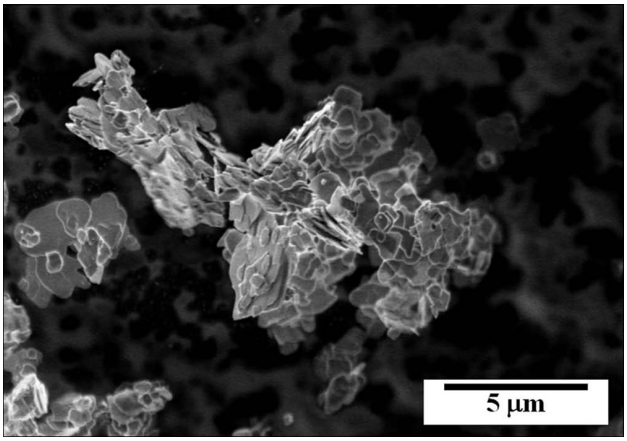

Fig. 3: Representative electron micrograph of as-prepared $La_2(CO_3)_3{\cdot}xH_2O$ starting powder.

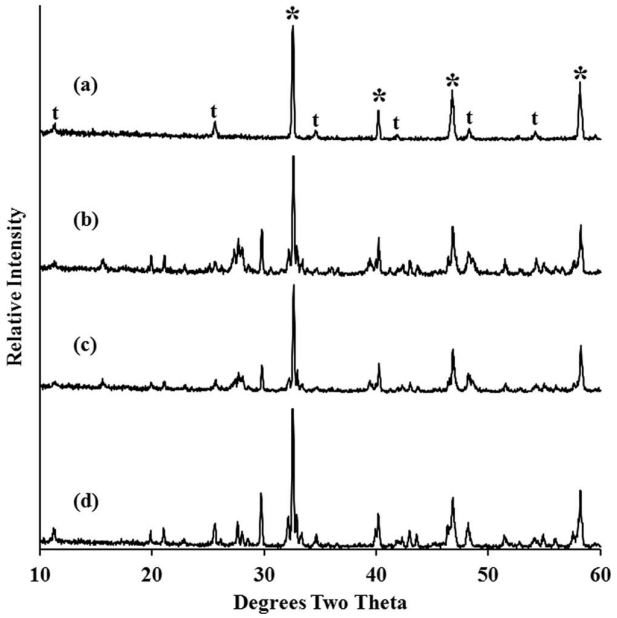

Fig. 4: X-ray diffraction patterns of LLTO, x = 0.097, calcined at 1100 °C for 1 h prepared from (a) $La_2(CO_3)_3{\cdot}xH_2O$; (b) $La(OH)_3$; (c) $La(OH)_2(NO_3){\cdot}xH_2O$; and (d) La_2O_3. The (a) pattern contains peaks solely from LLTO ("*" marks peaks shared by the cubic and tetragonal cells; "t" marks peaks due to the tetragonal superstructure) whereas the other patterns also contain mixtures of $La_2Ti_2O_7$, $Li_2Ti_3O_7$, and $La(OH)_3$.

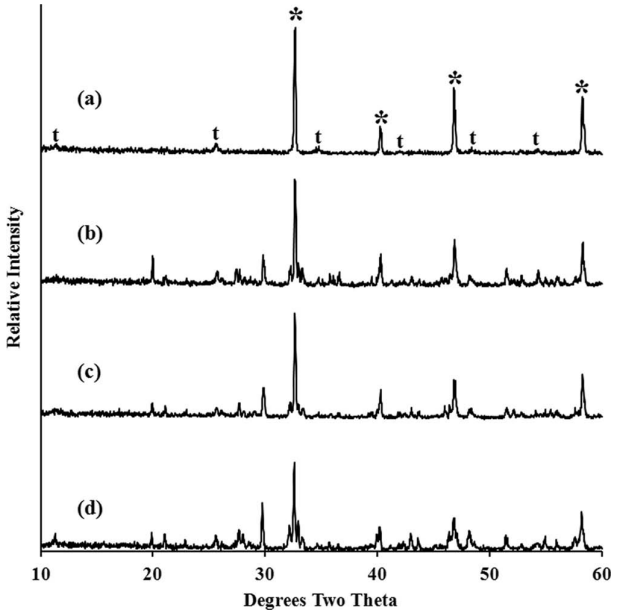

Fig. 5: X-ray diffraction patterns of LLTO, x = 0.117, calcined at 1100 °C for 1 h prepared from (a) $La_2(CO_3)_3{\cdot}xH_2O$; (b) $La(OH)_3$; (c) $La(OH)_2(NO_3){\cdot}xH_2O$; and (d) La_2O_3. The (a) pattern contains peaks solely from LLTO ("*" marks peaks shared by the cubic and tetragonal cells; "t" marks peaks due to the tetragonal superstructure) whereas the other patterns also contain mixtures of $La_2Ti_2O_7$, $Li_2Ti_3O_7$, and $La(OH)_3$.

As described in the procedures section, two compositions of LLTO were prepared using each of the La-starting materials. Figs. 4 and 5 show the XRD patterns of powders calcined at 1100 °C for 1 h for the entire series for $Li_{0.29}La_{0.57}TiO_3$ (x = 0.097) and $Li_{0.35}La_{0.55}TiO_3$ (x = 0.117), respectively. For both formulations, the LLTO prepared using $La_2(CO_3)_3{\cdot}xH_2O$ (Figs. 4a and 5a) exhibited near total conversion to the tetragonal LLTO super-

structure; neither unreacted starting materials nor side products were observed. Note that it is the observation of the smaller superstructure peaks (marked "t") that confirms the presence of the tetragonal superstructure [Space Group *P4/mmm*; PDF# 53 – 109]. The higher intensity peaks (marked "*") are shared by both the tetragonal and cubic cells, so it is the absence of the tetragonal superstructure peaks which would indicate a high degree of LLTO stabilized in the cubic structure [Space Group *Pm-3m*; PDF# 46 – 465]. Each of the other starting materials exhibited only partial conversion to the final product; in addition to LLTO diffraction peaks, each product contains varying degrees of the intermediate phases $La_2Ti_2O_7$ and $Li_2Ti_3O_7$ and residual unreacted $La(OH)_3$ (which was presumably originally present in the calcined mixture as La_2O_3 but formed via hydration on standing). Table 2 shows the measured surface area and size distributions of the calcined powders. While the surface areas were similar from sample to sample, the light scattering measurements revealed broad differences in agglomerate size distribution, which were generally confirmed by direct observation using SEM. A typical micrograph of x = 0.117 prepared from $La(OH)_3$ is given in Fig. 6, showing an approximate 20 μm agglomerate in which large pores and a highly necked morphology are evident. This is consistent with the D_{50} measured for this sample of 24.9 μm. Fig. 7 shows a representative SEM of the same LLTO formulation prepared from $La_2(CO_3)_3{\cdot}xH_2O$; agglomerates can be seen which are 10s of μm in diameter, but there is also a significant population of either smaller agglomerates or unagglomerated individual particles. This may be an indirect indication that this starting material forms a looser agglomerate structure on calcining which could be milled to finer particle size with relatively little effort.

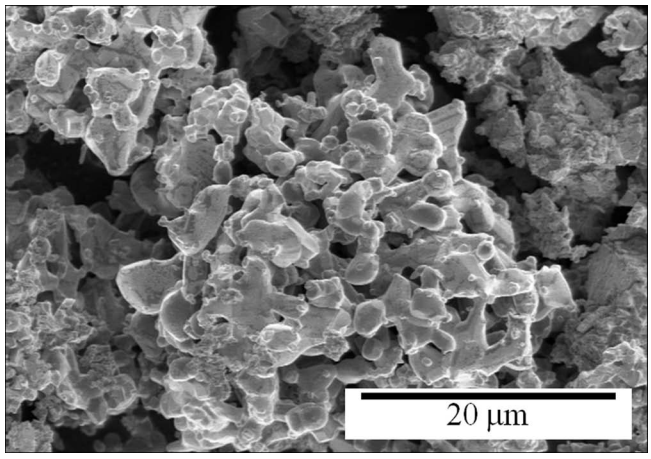

Fig. 6: Representative electron micrograph of LLTO calcined powder, x = 0.117, prepared using $La(OH)_3$.

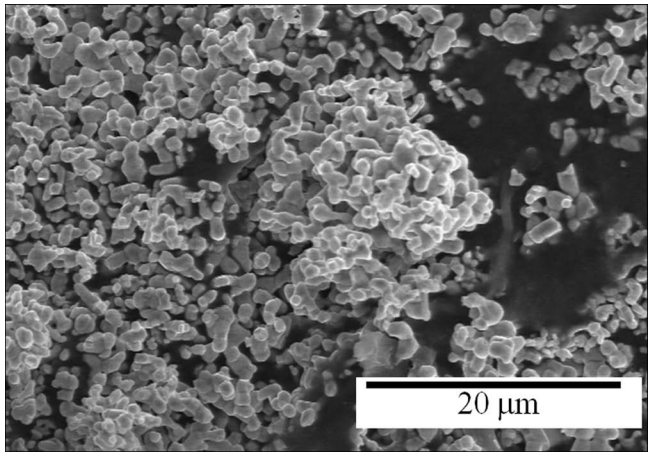

Fig. 7: Representative electron micrograph of LLTO calcined powder, x = 0.117, prepared using $La_2(CO_3)_3{\cdot}xH_2O$.

Table 2: Measured surface area and particle size distributions of $Li_{3x}La_{2/3-x}TiO_3$ (x=0.097 or 0.117) from different La starting materials.

La staring material	x	Surface area /m^2/g	Size distribution by dynamic light scattering	
			D_{50}/μm	D_{90}/μm
$La_2(CO_3)_3{\cdot}8H_2O$	0.097	2.15 ± 0.12	4.7 ± 0.2	36.2 ± 2.1
	0.117	1.34 ± 0.22	3.0 ± 0.1	8.3 ± 1.7
$La(OH)_3$	0.097	1.96 ± 0.03	30.5 ± 1.8	76.6 ± 12.5
	0.117	2.02 ± 0.34	24.9 ± 13.6	73.7 ± 36.7
$La(OH)_2(NO_3){\cdot}\ xH_2O$	0.097	1.93 ± 0.02	45.7 ± 1.1	95.9 ± 0.4
	0.117	2.14 ± 0.60	8.0 ± 0.7	26.7 ± 4.8
La_2O_3	0.097	1.43 ± 0.02	10.2 ± 0.5	24.2 ± 1.6
	0.117	4.16 ± 0.02	1.3 ± 0.2	2.7 ± 0.1

For use as an impermeable ceramic electrolyte, sintering of LLTO to near full density is required both for maximum ceramic strength and to maintain the integrity of the electrochemical boundary. The bulk densities measured for sintered parts from the current LLTO powders are given in Fig. 8. As no further particle size refinement on the as-calcined powders were performed, these results serve as an indication as to which of the formulations holds the most promise for further sintering optimization. The highest bulk densities are achieved for samples prepared from either $La_2(CO_3)_3{\cdot}xH_2O$ or La_2O_3. Theoretical full density for LLTO is ~5.0 g/cm³ (depending modestly on the relative amounts of tetragonal/cubic superstructure formation) so these values represent 90 – 95 % of full density. The samples prepared using hydroxide-containing La starting materials generally remained below this level of density.

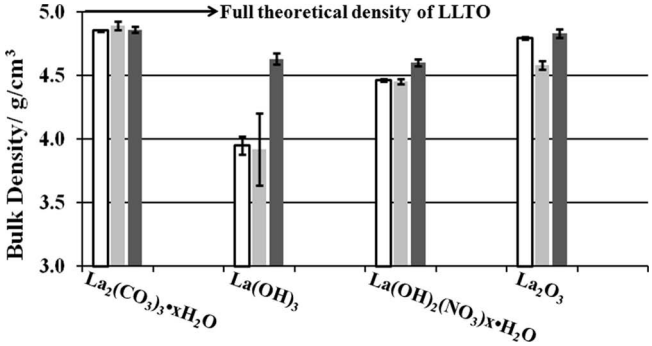

Fig. 8: Bulk densities of sintered LLTO prepared from different starting materials (white bar: x = 0.097 sintered at 1200 °C; light gray bar: x = 0.117 sintered at 1200 °C; dark gray bar: x = 0.117 sintered at 1300 °C).

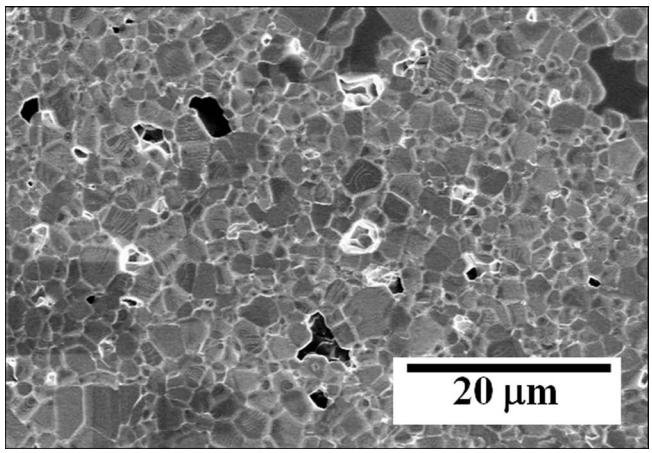

Fig. 9: Representative electron micrograph of a polished and etched surface of LLTO, x = 0.117, prepared using $La_2(CO_3)_3{\cdot}xH_2O$ sintered at 1200 °C.

The grain structure of sintered LLTO was investigated with electron microscopy on samples polished to 0.25 micron finish with diamond slurry and thermally etched at 1000 °C for 1 h. A representative view of the x = 0.117 LLTO sintered at 1200 °C using $La_2(CO_3)_3{\cdot}xH_2O$ is given in Fig. 9. Residual porosity is easily located in these and other samples, and the average grain size, calculated using the standard linear intercept method [23], is 3.1 ± 0.2μm. When sintered at 1300 °C, the grain size increases to 8.6 ± 0.1μm. Samples of x = 0.117 LLTO prepared using La_2O_3 have a similar average grain size (3.4 ± 0.1 mm) to that of the comparable $La_2(CO_3)_3{\cdot}xH_2O$-derived sample, but there are also isolated examples of grains much larger than the average (Fig. 10). When the sintering temperature is increased to 1300 °C, the size and occurrence of these larger grains increase, and the average size becomes 18.0 ± 4.0μm. As with the bulk density, LLTO prepared from either of the hydroxide-containing La-starting materials is notably different in microstructure from either the carbonate or oxide source. At 1200 °C the grains have a glassy appearance with few clear grain boundaries. When sintered at 1300°°C, the grain boundaries become more well defined, and similar average grain sizes of 11.2 ± 0.6μm and 10.4 ± 0.4μm were determined for x = 0.117 LLTO prepared from $La(OH)_3$ and $La(OH)_2(NO_3){\cdot}xH_2O$, respectively.

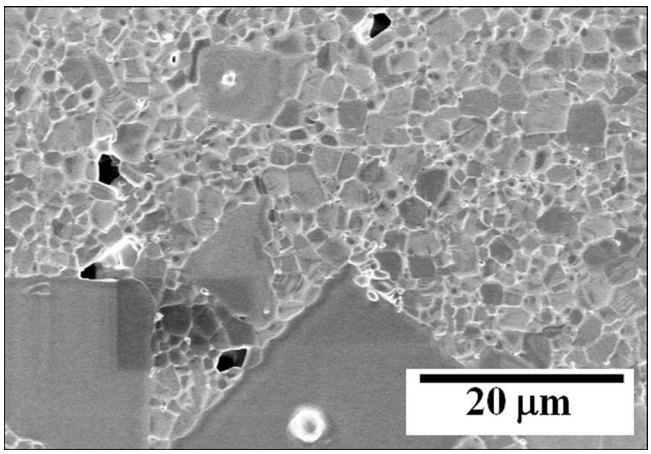

Fig. 10: Representative electron micrograph of a polished and etched surface of LLTO, x = 0.117, prepared using La_2O_3 sintered at 1200 °C.

The LLTO structure which formed after sintering showed a dependence on the La source material, composition, and sintering temperature. Fig. 11 shows the XRD's of x = 0.097 LLTO prepared from different La-sources and sintered at 1200 °C. Under these conditions, the different samples have actually all progressed to a similar LLTO structure on sintering. Second phases have been largely eliminated, and the diffraction patterns show major peaks which are shared by both the cubic and tetragonal superstructures (labeled with "*" in Fig. 10a) and the characteristic weaker peaks that are associated solely with the A-site ordering of Li^+ and La^{3+} cations which gives rise to the tetragonal superstructure (labeled "t" in Fig. 10a). The degree of ordering, as estimated from the relative intensity of these peaks [24] appears similar despite the different starting materials. Increasing the Li content (that is, increasing x to 0.117) causes notable changes to the phase formation on sintering at 1200 °C as seen by the XRD patterns shown in Fig. 12. Neither hydroxide-containing La-source has produced a phase-pure product; although diminished from their levels in the calcined powders, diffraction peaks primarily

of $La_2Ti_2O_7$ are clearly still present. Both La_2O_3 and the La carbonate have not only maintained full conversion to LLTO, but the intensity of the tetragonal superstructure lines is greatly diminished. In the case of LLTO from $La_2(CO_3)_3{\cdot}xH_2O$, the tetragonal superstructure lines are not detectable. It is well known that for $0.11 < x < 0.12$, the cubic character of the LLTO superstructure is enhanced but typically not in the absence of rapid quenching from a sintering temperature > 1150 °C [13]. Even low-temperature methods in which disorder on the A-site could be more probable due to kinetic effects have been shown to result in a significant degree of tetragonal superstructure formation due to cation ordering [19]. The tendency for cubic LLTO formation when using $La_2(CO_3)_3{\cdot}xH_2O$ is diminished when the sintering temperature is increased to 1300 °C, and weak tetragonal peaks are now observed with XRD (Fig. 13). The rates of cation ordering which lead to increased amounts of tetragonal superstructure have been shown to vary with annealing temperature as well as quenching rates [24]. In the current examples of LLTO prepared from $La_2(CO_3)_3{\cdot}xH_2O$, sintering at 1300 °C apparently provides enough residual thermal energy on cooling to promote the Li^+/La^{3+} ordering, which gives rise to the tetragonal superstructure whereas sintering at 1200 °C does not. For the hydroxide-based formulations, the increased temperature has removed the residual intermediate phases which were present when sintered at 1200 °C, and the LLTO that results exhibits peaks characteristic of the tetragonal superstructure. The LLTO prepared with La_2O_3 exhibits a similar degree of tetragonal ordering to that of the hydroxide-derived LLTO.

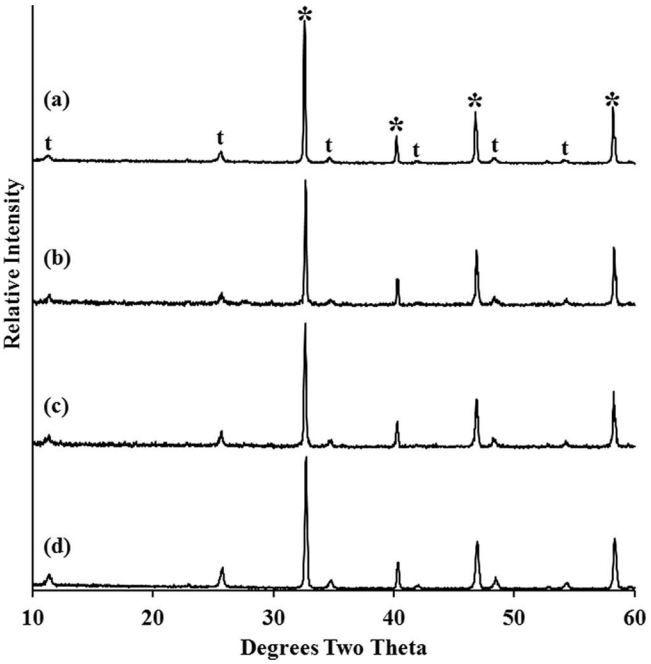

Fig. 11: X-ray diffraction patterns of LLTO, x = 0.097, sintered at 1200 °C for 5 h prepared from (a) $La_2(CO_3)_3{\cdot}xH_2O$; (b) $La(OH)_3$; (c) $La(OH)_2(NO_3){\cdot}xH_2O$; and (d) La_2O_3. Peaks labeled with "*" are shared by the cubic and tetragonal unit cells, and peaks labeled with "**t**" are solely due to the tetragonal superstructure.

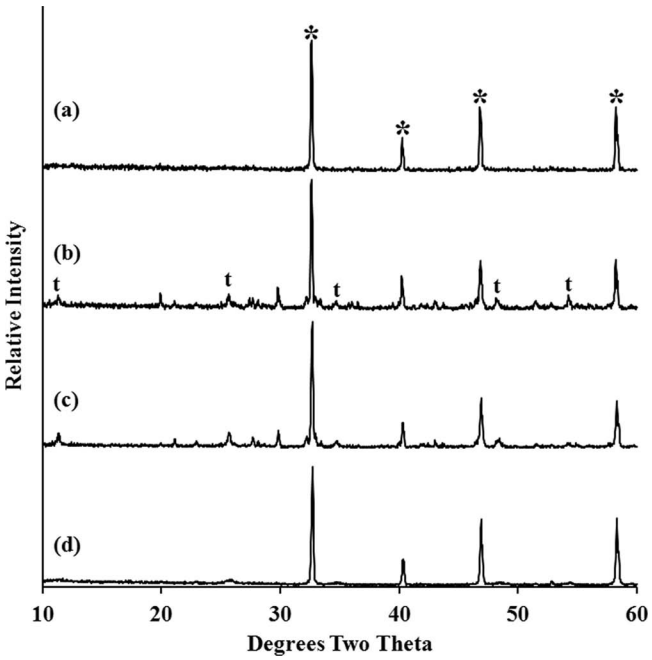

Fig. 12: X-ray diffraction patterns of LLTO, x = 0.117, sintered at 1200 °C for 5 h prepared from (a) $La_2(CO_3)_3{\cdot}xH_2O$; (b) $La(OH)_3$; (c) $La(OH)_2(NO_3){\cdot}xH_2O$; and (d) La_2O_3. Peaks labeled with "*" are shared by the cubic and tetragonal unit cells, and peaks labeled with "**t**" are solely due to the tetragonal superstructure.

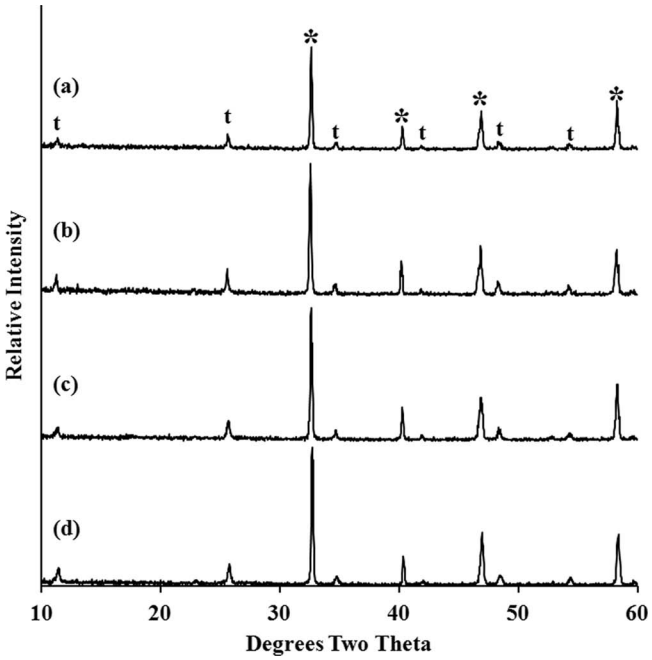

Fig. 13: X-ray diffraction patterns of LLTO, x = 0.117, sintered at 1300 °C for 5 h prepared from (a) $La_2(CO_3)_3{\cdot}xH_2O$; (b) $La(OH)_3$; (c) $La(OH)_2(NO_3){\cdot}xH_2O$; and (d) La_2O_3. Peaks labeled with "*" are shared by the cubic and tetragonal unit cells, and peaks labeled with "**t**" are solely due to the tetragonal superstructure.

It is generally accepted that LLTO with higher degrees of A-site cation disorder (i.e. with a higher degree of cubic character to the superstructure ordering) will tend toward higher values of lattice ionic conductivity [13,24]. Similar behavior is observed in this current study, and measured values of lattice conductivity for the various samples are given in Fig. 14. LLTO prepared using $La_2(CO_3)_3{\cdot}xH_2O$ exhibits both higher degrees of cubic superstructure and

higher levels of Li^+ lattice conductivity than samples prepared with other La starting materials for a given set of compositions and sintering conditions. In fact, the highest value of $1.46 \pm 0.28 \cdot 10^{-3}$ S/cm is achieved for LLTO prepared using the La carbonate source with x = 0.117 and sintered at 1200 °C, which had no tetragonal superstructure detectable with XRD. Lattice conductivity values for the other samples from this starting material were close to $1.0 \cdot 10^{-3}$ S/cm, a value comparable to the highest reported literature values [13]. The next highest overall lattice conductivities were measured for La_2O_3-derived samples, and decreasing values of lattice conductivity seem to follow roughly with the amount of hydroxide in the starting material. Note that the samples for x = 0.097 sintered at 1200 °C using $La(OH)_2(NO_3) \cdot xH_2O$ were fragile due to low density and crumbled during preparation for the conductivity measurement. Interestingly, the magnitude of the lattice conductivity seems to follow the same general trend as did the bulk density, with carbonate starting materials having the highest bulk density, followed by La_2O_3, $La(OH)_2(NO_3) \cdot xH_2O$, and finally $La(OH)_3$. This suggests that in addition to the concerns regarding reproducible stoichiometric control described in the introduction, detrimental effects on densification and lattice conductivity may also arise from the presence of hydroxide contamination of La_2O_3 starting material.

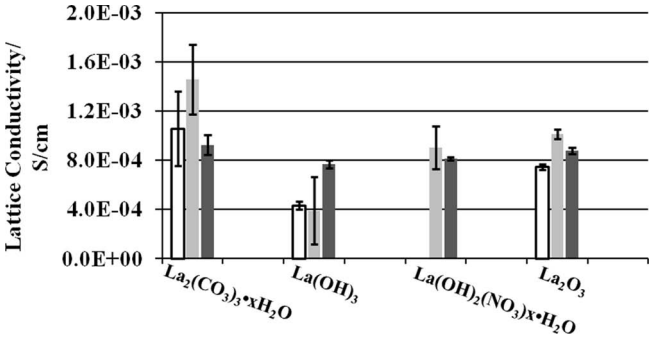

Fig. 14: Lattice Li^+-conductivity of sintered LLTO prepared from different starting materials (white bar: x = 0.097 sintered at 1200 °C; light gray bar: x = 0.117 sintered at 1200 °C; dark gray bar: x = 0.117 sintered at 1300 °C).

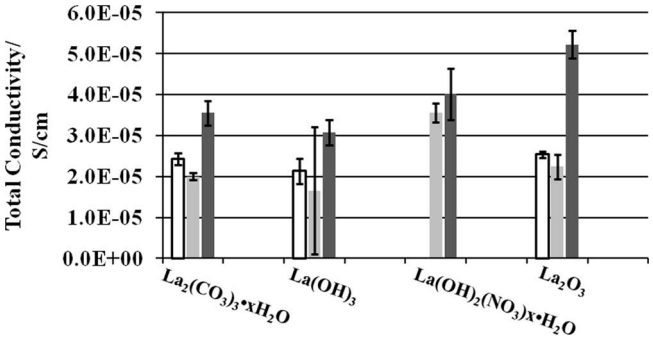

Fig. 15: Total Li^+-conductivity of sintered LLTO prepared from different starting materials (white bar: x = 0.097 sintered at 1200 °C; light gray bar: x = 0.117 sintered at 1200 °C; dark gray bar: x = 0.117 sintered at 1300 °C).

The total Li^+ conductivity, that is the conductivity across the entire sample including grain boundary resistance, is given in Fig. 15. Except for one anomalously high and one anomalously low measurement, the samples all exhibit values between $2.0 \cdot 10^{-5}$ and $4.0 \cdot 10^{-5}$ S/cm. For use as a solid electrolyte, the total conductivity should be as close to the lattice conductivity as possible, with a value of $1.0 \cdot 10^{-4}$ S/cm being a minimum value for promising device testing. Total conductivity most closely depends on features of the ceramic microstructure such as grain size [25], residual porosity [26] and grain boundary phases [27]. The similar values observed here indicate that the total conductivity is independent of the La starting materials surveyed.

IV. Summary and Conclusions

Of the La starting materials investigated in this study, $La_2(CO_3)_3 \cdot xH_2O$ appears to offer several advantages for the synthesis and sintering of LLTO ceramics. First, powders synthesized from this material consistently produced a product that was fully reacted to LLTO after calcination at 1100 °C for 1 h, whereas the other starting materials all exhibited some degree of residual intermediate phases under similar conditions. It is not unreasonable to speculate that the higher phase homogeneity of $La_2(CO_3)_3 \cdot xH_2O$-derived LLTO also played a favorable role in promoting more uniform densification during sintering of this powder, leading to the some of the highest bulk densities of this study. Additionally, the carbonate-derived LLTO showed consistent and complete formation of phase-pure LLTO after sintering, and when the x = 0.117 composition was sintered at 1200 °C, there was a marked decrease in the formation of tetragonal superstructure. Lastly, $La_2(CO_3)_3 \cdot xH_2O$ resulted in sintered LLTO which consistently had the highest lattice conductivity of the surveyed starting materials sintered under similar conditions. The presence of hydroxide in the La starting material appears to have been detrimental to several properties including bulk density and lattice conductivity. In order to fully exploit these observations, further control experiments are necessary to clearly understand the mechanistic consequences of using $La_2(CO_3)_3 \cdot xH_2O$ for the synthesis of LLTO; however, our current results are sufficiently positive that this material will be the focus of additional optimization and device development.

References

1 Lee, J.-S., Kim, S.T., Cao, R., Choi, N.-S., Lui, M., Lee, K.T., Cho, J.: Metal-air batteries with high energy Density: Li-air versus Zn-air, *Adv. Energy Mater.*, **1**, 34 – 50, (2011).

2 Kraytsberg, A., Ein-Eli, Y., Review on Li-air batteries – opportunities, limitations, and perspective, *J. Power Sources*, **196**, 886 – 893, (2011).

3 Kumar, B., Kumar, J., Leese, R., Fellner, J.P., Rodrigues, S.L., Abraham, K.M.: A solid-state, rechargeable, long cycle life lithium-air battery, *J. Electrochem. Soc.*, **157**, A50 – A54, (2010).

4 Abraham, K.M., Jiang, Z.: A polymer electrolyte-based rechargeable Lithium/Oxygen battery, *J. Electrochem. Soc.*, **143**, 1 – 5, (1996).

5 Abraham, K.M., Jiang, Z., Carroll, B.: Highly conductive PEO-like polymer electrolytes, *Chem. Mater.*, **9**, 1978 – 1988, (1997).

6 Kuboki, T., Okayama, T., Ohsaki, T., Takami, N.: Lithium-air batteries using hydrophobic room temperature ionic liquid electrolyte, *J. Power Sources*, **146**, 766 – 769, (2005).

7 Visco, S.J., Katz, B.D., Nimon, Y.S., DeJonghe, L.C.: Protected active metal electrode and battery cell structures with non-aqueous interlayer architecture, U.S. Patent 7,282, 295 B2, (2007).

8 Kowaluk, I., Read, J., Salomon, M.: Li-air batteries: A classic example of limitations owing to solubilities, *Pure Appl. Chem.*, **79**, 851 – 860, (2007).

9 Wolfenstine, J., Allen, J.L.: Reaction of $Li_{0.33}La_{0.57}TiO_3$ with water, *J. Mater. Sci.*, **43**, 7247 – 7249, (2008).

10 Kotobuki, M., Suzuki, Y., Munakata, H., Kanamura, K., Sato, Y., Yamamoto, K., Yoshida, T.: Compatibility of $LiCoO_2$ and $LiMn_2O_4$ cathode materials for $Li_{0.55}La_{0.35}TiO_3$ electrolyte to fabricate all-solid-state lithium battery, *J. Power Sources*, **195**, 5784 – 5788, (2010).

11 OudenHoven, J.F.M., Baggetto, L., Notten, P.H.L.: All-Solid-state lithium-ion Microbatteries: A review of various three-dimensional concepts, *Adv. Energy Mater.*, **1**, 10 – 33, (2011).

12 Inaguma, Y., Liquan, C., Itoh, M., Nakamura, T., Uchida, T., Ikuta, H., Wakihara, M.: High ionic conductivity in lithium lanthanum titanate, *Solid State Commun.*, **86**, 689 – 693, (1993).

13 Stramare, S., Thangadurai, V., Weppner, W.: Lithium lanthanum titanates: A review, *Chem. Mater.*, **15**, 3974 – 3990, (2003).

14 Inaguma, Y., Chen, L., Itoh, M., Nakamura, T.: Candidate compounds with perovskite structure for high lithium ionic conductivity, *Solid State Ionics*, **70/71**, 196 – 202, (1994).

15 Harada, Y., Ishigaki, T., Kawai, H., Kuwano, J.: Lithium ion conductivity of polycrystalline perovskite $La_{0.67-x}Li_{3x}TiO_3$ with ordered and disordered arrangements of the A-site ions, *Solid State Ionics*, **108**, 407 – 413, (1998).

16 Sutorik, A.C., Green, M.D., Cooper, C., Wolfenstine, J., Gilde, G.: The comparative influences of structural ordering, grain size, Li-content, and bulk density on the Li^+-conductivity of $Li_{0.29}La_{0.57}TiO_3$, *J. Mater. Sci.*, **47**, 6992 – 7002, (2012).

17 Wöhrle, T., Gomez-Romero, P., Fries, T., West, K., Palacin, M.R., Casan-Pastor, N.: Sol-gel synthesis of the lithium ion conducting perovskite $La_{0.57}Li_{0.3}TiO_3$: effect of synthesis and thermal treatments on the structure and conducting properties, *Ionics*, **2**, 442 – 445, (1996).

18 Kitaoka, K., Kozuka, H., Hashimoto, T., Yoko, T.: Preparation of $La_{0.5}Li_{0.5}TiO_3$ perovskite thin films by the sol-gel method, *J. Mater. Sci.*, **32**, 2063 – 2070, (1997).

19 Pham, Q.N., Bohnké, C., Crosnier-Lopez, M.-P., Bohnké, O.: Synthesis and characterization of nanostructure fast ionic conductor $Li_{0.30}La_{0.56}TiO_3$, *Chem. Mater.*, **18**, 4385 – 4392, (2006).

20 Shin, J.-W., Hong, C.-H., Yoon, D.-H.: Effects of TiO_2 starting materials on the solid -state formation of $Li_4Ti_5O_{12}$, *J. Am. Ceram. Soc.*, **95**, 1894 – 1900, (2012).

21 Bauerle, J.E.: Study of solid electrolyte polarization by a complex admittance method, *J. Phys. Chem. Solids*, **30**, 2657 – 2670, (1969).

22 Huggins, R.A.: Simple method to determine electronic and ionic components of the conductivity in mixed conductors: A review, *Ionics*, **8**, 300 – 313, (2002).

23 Wurst, J.C., Nelson, J.A.: Lineal intercept technique for measuring grain size in two-phase polycrystalline ceramics, *J. Am. Ceram. Soc.*, **55**, 109, (1972).

24 Harada, Y., Hirakoso, Y., Kawai, H., Kuwano, J.: Order-disorder of the A-site ions and lithium ion conductivity in the perovskite solid solution $La_{0.67-x}Li_{3x}TiO_3$, *Solid State Ionics*, **121**, 245 – 251, (1999).

25 Ban, C.W., Choi, G.M.: The effect of sintering on the grain boundary conductivity of lithium lanthanum titanates, *Solid State Ionics*, **140**, 285 – 292, (2001).

26 Thangadurai, V., Weppner, W.: Recent progress in solid oxide and lithium ion conducting electrolytes research, *Ionics*, **12**, 81 – 92, (2006).

27 Mei, A., Wang, X.-L., Lan, J.-L., Feng, Y.-C., Gen, H.-X, Lin, Y.-H., Nan, C.-W.: Role of amorphous boundary layer in enhancing ionic conductivity of lithium-lanthanum-titanate electrolyte, *Electrochim. Acta.*, **55**, 2958 – 2963, (2010).